

Failure of the vacuum in a vacuum insulated hose while flowing liquid hydrogen

Richard Goff, Andrew Newton, Greg Wray, Wayne Rattigan, Janni Vizma and Kieran Lyons

HSE Science and Research Centre, Buxton, Derbyshire, UK. SK17 9JN

Liquid hydrogen (LH_2) is being introduced as a fuel source for transportation that is carbon free at the point of use as part of the drive to Net Zero. LH_2 has higher densities than even high-pressure hydrogen gas at ambient temperature (the density of LH_2 is 71 kg m^{-3} compared to 40 kg m^{-3} for gas at 293 K and 700 barg).

Due to the low boiling point of LH_2 (approximately 20 K), high levels of insulation are required to reduce heat ingress during storage and transport. Super insulated vacuum lines (SIVL) contain multi-layer insulation (MLI) and a high vacuum to reduce heat transfer. Vacuum failure causes the $LH_2$to warm due to the increased heat transfer caused by the presence of air in the vacuum cavity. Condensation and freezing of air cause the heat transfer to rise significantly.

HSE were performing experiments with LH_2 for the ZEST (Zero Emissions for Sustainable Transport) programme when the failure of the vacuum in a SIVL hose occurred. The hose was the main transfer link from the LH_2 supply trailer to the release station. This paper looks at the failure of this SIVL hose.

The cause of the vacuum failure was attributed to a cryogenic leak from a bespoke mass flow measurement system with 1.5" LH_2 Linde bayonet fittings. The leak impinged into the vicinity of the vacuum plug cooling the skin of the hose and leading to contraction and subsequent plug failure. The possible causes of the seal failure are discussed, and the effects this had on the propensity for ongoing leakage is explored.

The flow characteristics of the cryogenic hydrogen within the hose are also discussed. A temperature and pressure rise of 2 K and 0.7 barg in the hose were recorded following the loss of vacuum. There was a discernible drop in the mass flow of the liquid after the vacuum failed and an estimation of the leakage rate of the LH_2 from the system is provided. The heat transfer rate to the hydrogen and the vapour fraction after vacuum loss were estimated.

Based on this, the hazard distances are quantified and compared with existing safety guidance for such unexpected releases.

Introduction

Liquid hydrogen (LH_2) is being introduced as a fuel source for transportation that is carbon free at the point of use as part of the drive to Net Zero. LH_2 has higher densities than even high-pressure hydrogen gas at ambient temperature (the density of LH_2 is 71 kg m^{-3} compared to 40 kg m^{-3} for gas at 293 K and 700 barg (NIST, 2023)).

Due to the low boiling point of LH_2 (approximately 20 K), it needs to be stored and transported using high levels of insulation to reduce heat ingress. Super insulated vacuum lines (SIVL) contain a high vacuum to reduce heat transfer. Vacuum failure will result in increased heat transfer to the LH_2, both from condensation of the air that has leaked into the vacuum space and from the increased thermal conductivity without the vacuum.

This paper describes the failure of a vacuum in a flexible SIVL (also known as a vacuum insulated hose) during the transfer of LH_2. This failure occurred while HSE Science and Research Centre were performing experiments for the ZEST (Zero Emissions for Sustainable Transport) programme. The vacuum insulated hose was 20 m long and connected to a mass flow meter with a 1.5" Linde bayonet. The hose comprised a 25 mm inner hose surrounded by 30 layers of Multi-Layer Insulation (MLI), which was contained within a 65 mm diameter outer hose. The region with the MLI had a vacuum which was generated through two vacuum ports, one at each end of the hose. The vacuum ports contained a brass vacuum plug located at the end of a stainless-steel stalk, which were protected by a black rubber dust cover.

The authors of this paper have only found one previous account of a vacuum loss in a flexible SIVL (Demko, 2008). In this case, this was a deliberate vacuum loss during experiments transferring liquid nitrogen (LN_2). Temperature rises between 1.5 and 6 K were observed during those experiments, which corresponded to a heat flux to the flowing nitrogen of between 0.7 and 2.2 kW m^{-2}, the higher values being for experiments with subcooling (this will allow for condensation of nitrogen and oxygen from the air, rather than just oxygen when the LN_2 was not subcooled). The analyses during these experiments did not account for evaporation of LN_2 in their calculations of the heat transfer, so may be underestimating it. During experiments without subcooling of the liquid nitrogen supply, the nitrogen temperature was above the saturation temperature and pressure after the loss of vacuum. Modest pressure rises of less than 0.1 barg were seen for experiments with subcooled LN_2, which raised the temperature to the saturation point of nitrogen. Temperatures on the outside and in the middle of the MLI dropped after loss of vacuum due to increased thermal conductivity in the presence of air but rose on the inner layer of the MLI.

MLI has alternating layers of a reflective layer such as aluminium foil and an insulating spacer layer such as glass fibre tissue, as shown in Figure 1. Each pair is referred to as one layer. The reflective layer limits radiation transfer while the insulating spacer layer limits thermal conductivity from one reflective layer to another. A high vacuum (0.1 Pa or less) is required to prevent convection from the outer to inner skin of the vessel. The heat flux/thermal conductivity across space increases rapidly above this pressure, above 100 Pa the increase in thermal conductivity starts to saturate at a value at least two orders of magnitude greater (Fesmire (2018), Funke (2015) and Sun (2009)).

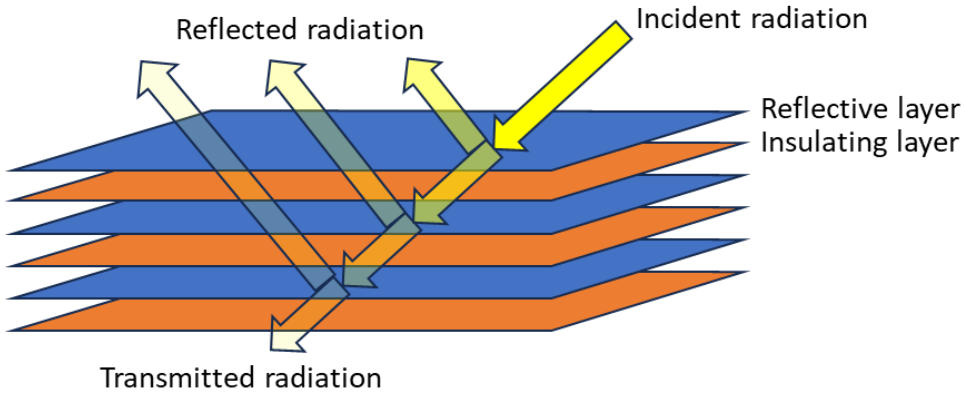

Figure 1: A simplified diagram showing how MLI prevents transfer of radiation across the vacuum space in SIVL. Secondary radiation reflections within the MLI are not shown for ease of understanding

Timeline of events

An overview of the key events that occured during the incident are given in the timeline below using times after the start of the experiment:

- 15 s – liquid hydrogen first allowed into pipework and hoses, which started cooling them down
- ≈ 150 s – fluid flowing through the mass flow meter and entering the 20 m vacuum hose becomes liquid (as evidenced by mass flow and drive gain on Coriolis mass flow meter)
- ≈ 250 s – fluid flow in release station becomes (mostly) liquid (as evidenced by temperature measurements)
- 291 s – Small leak on upstream joint begins.
- 425 s – Leak on downstream joint begins.
- 429 s – Downtream leak progresses to large leak. Mass flow rate increases by 25 g s^{-1}.
- ≈ 550 s – Vacuum insulation fails – Mass flow rate lowers, pressure and temperature rise.

Figure 2, Figure 3 and Figure 4 show images taken of the leaks around the Coriolis mass flow meter at 291 s, 425 s, and 491 s after the start of the experiment respectively, with Figure 5 being taken after the experiment.

At 291 s into the experiment, a small leak occurred on the upstream side joint (see Figure 2Figure 3). This leak progressed slowly and had not grown significantly larger by the time a leak started on the downstream joint (see Figure 4). The flow downwards towards the ground from the upstream joint is believed to be condensation of air from the external wall that had been cooled by the LH_2 leak; this fluid could be seen to have lower momentum than the LH_2 leaving the joints. Within 4 s, the leak from the downstream joint had progressed rapidly into a large leak (see Figure 4). This leak on the downstream side can be seen to be several leaks that occurred around the circumference of the joint. The leak(s) occur below a clamp, and this appears to split the leak(s) into two and remove some of the momentum of the release. The release quickly gained buoyancy as it slowed down and warmed up (likely to be from contact with both the clamp and the air). The release of LH_2 was impinging on and cooling down the stalk that contained the vacuum port (the black rubber dust cover can be seen on it in Figure 2, Figure 3 and Figure 4. There was no hazard to people from the leak during this experiment as there was a 200 m exclusion zone in place.

Figure 5 shows the flow meter and joints after the experiments, ice was observed on the joints where they have been cooled and the vacuum plug is no longer in the port (the black rubber dust cover is missing). The vacuum plug was found on the floor, in the figure it is placed upon the frame and marked with a white arrow.

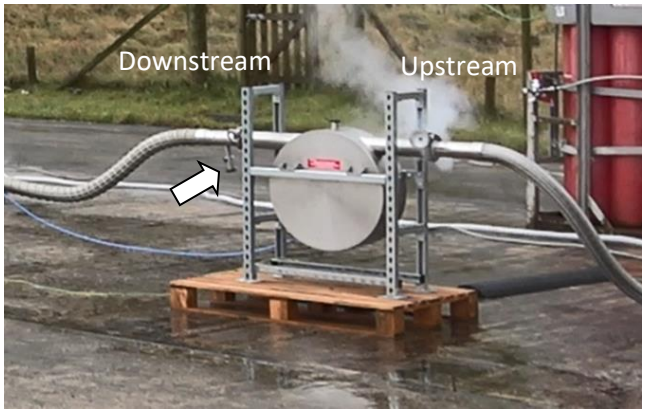

Figure 2: The initial small leak upstream of the flow meter. This occurred at 291 s into the experiment. The vacuum port is shown with an arrow, the upstream and downstream sides of the flow meter are labelled.

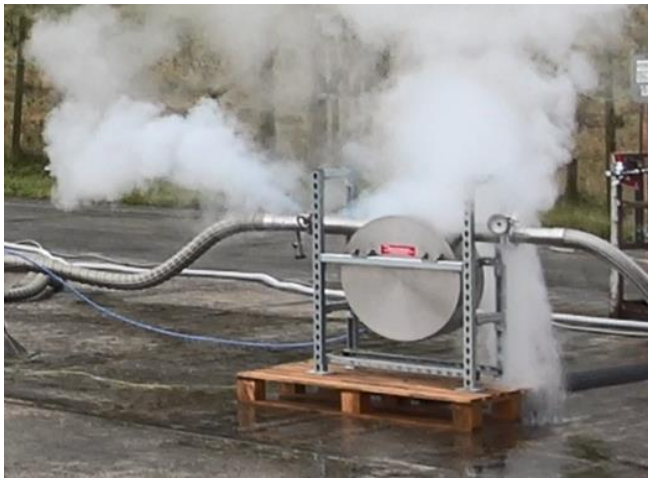

Figure 3: The start of the leak on the downstream side of the flowmeter, it can also be seen that the leak rate on the upstream side had increased. The flow downwards towards the ground from the upstream joint is believed to be condensation of air from the external wall that had been cooled by the LH_2 leak This occurred at 425 s into the experiment.

Figure 4: The leak on the upstream side of the flowmeter has progressed quickly to a large leak, it can be seen that it is impinging on the vacuum port of the hose. This occurred at 429 s into the experiment.

Figure 5: Ice can be seen on the joints of the hoses with the flowmeter after the experiment has finished. The vacuum plug is no longer in the port and is marked with the arrow on top of the frame

Cause of LH2 leak

Figure 6: The left picture shows a 1.5” Linde bayonet and the corresponding female port (note that these are not the bayonet and port pair that leaked, but are shown for illustration). The right picture shows two joints held in place by the clamp

At ambient temperature, the system was gas tight when tested with nitrogen and hydrogen. The leaks started when the system was cold due to the presence of LH_2. The 1.5” Linde bayonet and female port are shown in Figure 6, a rubber O-ring is put in the groove on the female port and the two pieces are held together with a clamp (also see Figure 6). During the leak, liquid/cold gaseous hydrogen will have passed both the PTFE sealing ring seen on the end of the bayonet and the rubber O-ring. The PTFE sealing ring touched on the inside wall of the female port and slid along when the joint was assembled. Liquid and/or cold gas would have passed into the space between the bayonet and the female port, the pressure in that space would have raised until fluid was released past the O-ring. It is likely that a leak path was created through differential contraction on cooling. The leaks were stopped in later experiments by placing a thicker O-ring in the groove between the face of the bayonet and female port.

The PTFE ring (at the cold end) is meant to prevent/limit liquid passing into the bayonet port, and the O-ring is meant to prevent relatively warm gas from leaving the port. Since this leak, we have found reports that bayonet fittings work best when angled downwards to help maintain the temperature gradient (Meyer Tool, undated). It is possible that there was misalignment of the hoses due to them being unsupported, which might have aided a liquid leak past the PTFE seal, so supporting the hose may have helped. A tolerance issue on the fittings is another possibility. Longer bayonets could have helped with maintaining that temperature difference, so also reduced the likelihood of a leak.

Data recorded

The data recorded during the experiment is shown in Figure 7 and Figure 8. The mass flow measurements were made immediately before the hose that lost its vacuum insulation, and the temperature and pressure were recorded in the release station at the end of the 20 m hose. The low value of the drive gain suggests that a single phase fluid was passing through the Coriolis mass flow meter, given the temperatures and pressures recorded it can be inferred that this was liquid. Analysis of the saturation temperature and pressure later in this paper will show that the fluid remained predominantly liquid in the release station after flowing through the hose while the vacuum insulation remained in place.

At 429 s when the large leak occurred in Figure 4, the mass flow in Figure 7 shows a jump of 25 g s^{-1}. At around 550 s, the mass flow suddenly drops, this corresponds to a change in pressure of 0.7 barg and temperature of 2 K. It can be inferred this is the point where the vacuum in the hose was lost.

After 600 s, the mass flow increases, the pressure continues to decrease at the same rate as before the vacuum loss and the temperature remains constant. The oscillations seen in the mass flow measurements are possibly an artifact of the way Coriolis flow meters work or could be related to cycles of gas flow and condensation within the outer hose. The pressure drops are caused by a dwindling source pressure from the LH_2 tanker driving the flow and was seen in all the experiments during this test campaign. The temperature remaining constant is indicative of the fluid being at its saturation temperature and pressure, this is discussed further in the next section.

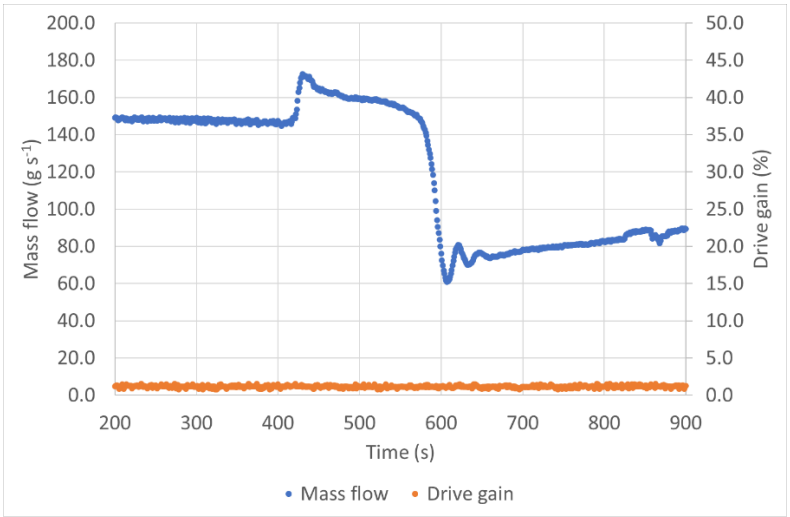

Figure 7: The mass flow measured during the experiment and the drive gain on the Coriolis meter

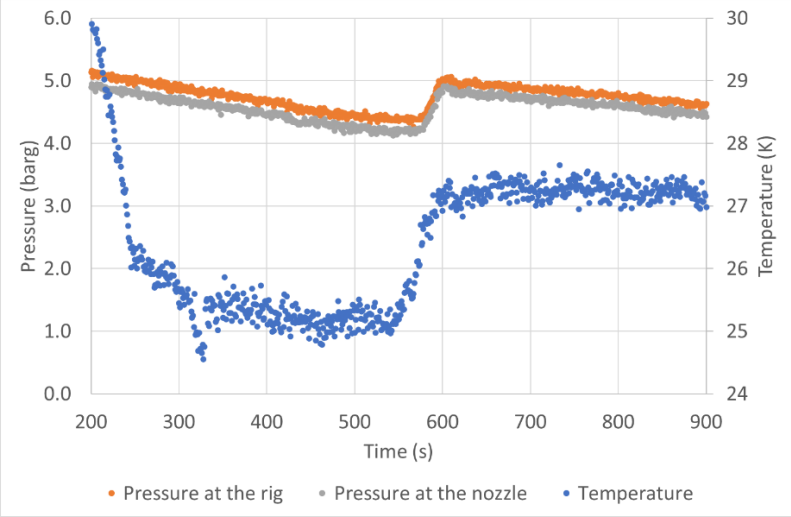

Figure 8: The temperature and pressure measured in the release station during the experiments

Analysis

The values of temperature and pressure recorded in the release station before and after vacuum loss are shown in Figure 9. These are compared to the saturation values obtained from CoolProp (Bell, 2014). The data points to the left are before the vacuum loss, and those to the right are after. The upwards slope of points follows the slope of the saturation curve from CoolProp (Bell, 2014) using the Helmholtz equation of state described in Leachman et al. (2009). This points to the fluid being at its saturation temperature and pressure once the vacuum has been lost. There is a 0.5 K discrepancy between the measured temperature/pressure at each point and those expected from CoolProp, this is a close agreement given the uncertainties in temperature and pressure measurement at such low temperatures.

Before the loss of vacuum, the fluid is below the saturation temperature at a given pressure, this is indicative that the fluid has remained predominantly liquid when it has reached the release station. The low drive gain on the Coriolis meter showed that it was liquid when it entered the vacuum hose. The drive gain is the amount of energy to oscillate the flow tubes to their resonant frequency, and is high when a multiphase fluid is present in the Coriolis meter (Weinstein, 2010). In Figure 9, the measured temperatures and pressures after the vacuum failure event is taken as evidence that the conditions of the fluid in the pipe are likely to be saturated and two-phase.

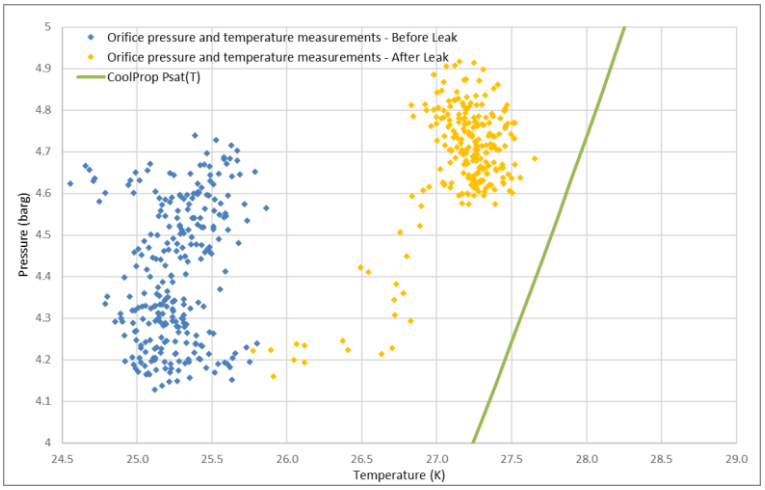

Figure 9: The temperatures and pressures recorded in the release station, and their comparison to the saturation values in CoolProp. The points on the left are before the vacuum loss, and those to the right are after the vacuum loss

The vacuum failure event was instrumented with the mass flow rate ($\dot{m}$), orifice pressure (P_{nozzle}) and temperature (T_{nozzle}) and release station (midway) pressure (P_{mid}). Analysis of these measurements enables the heat transfer coefficient to be estimated during a practical scenario. The following analysis assumes that the flow in the pipe is in steady state. The general one-dimensional momentum conservation equation is therefore:

$$\frac{dP}{dx} = -\frac{2f}{D_{\text{pipe}}\rho} G^2 \quad (1)$$

Where:

- f is the Fanning friction factor (-)
- D_{pipe} is the pipe diameter (m)
- ρ is the density along the pipe (kg m^{-3})
- G is the mass flux density (kg m$^{-2}s^{-1}$)
- x is the distance along the pipe (m)

Equation (1) is integrated assuming averaged quantities along the pipe, with the mass flux density being replaced by the mass flow rate ($\dot{m}$, kg s^{-1}) divided by the pipe area (A_{pipe}^2, m^2):

$$\Delta P = \frac{L_{pipe} 2f}{D_{pipe}\bar{\rho} A_{pipe}^2} \dot{m}^2 \quad (2)$$

Where in additional to the previously defined variables, L_{pipe} is the pipe length (m).

In the experiments, the pressure change was measured over a section of the pipe ($\Delta P = P_{\text{mid}} - P_{\text{nozzle}}$) as well as the mass flow rate ($\dot{m}$). The pipe average density ($\bar{\rho}$) can also be inferred from the temperature and pressure assuming that the fluid was fully liquid. Rearranging the pipe averaged momentum equation (2) reveals the following expression for (K_{fric}):

$$\frac{\bar{\rho}\Delta P}{\dot{m}^2} = \frac{L_{pipe} 2f}{D_{pipe} A_{pipe}^2} = K_{\text{fric}} \quad (3)$$

Rearranging (3) gives the following ratio that can be used to estimate the density before and after vacuum loss as the pipe configuration remained unchanged:

$$\bar{\rho} = \frac{K_{\text{fric}} \dot{m}^2}{\Delta P} \quad (4)$$

The average density for the flow between 200 and 400 s was used as a baseline for calculating the relative density before and after the vacuum loss. Note that the mass flow rate was estimated based on two different values for the leak (0 $g\ s^{-1}$ and 25 $g\ s^{-1}$). It was assumed in this analysis that the fluid in the release station before the vacuum loss was fully liquid. The vapour fraction after vacuum loss was calculated using the densities of the liquid and vapour at saturation. The results of these analyses are shown in Figure 10. The vapour fraction of the fluid entering the release station after loss of the vacuum is initially between 80% and 100% (the higher value has had 25 g s^{-1} subtracted from the measured LH_2 flow before calculating the relative density and vapour fraction, the lower value has no correction for the leak of LH_2). The vapour fraction reduces over time to between 55% and 85%; this suggests the heat flow into the hose has reduced as less liquid is evaporating. This increase in liquid volume fraction (volume of liquid in total volume) and hence density is the reason the mass flow was seen to increase in Figure 7.

Experience from other (as yet) unpublished experiments on a planned loss of vacuum on a LH_2 tank suggests that there would be a rapid air flow into the outer hose once the containment of the vacuum is breached, and this would settle to a significantly lower flow rate on a much shorter time scale than the drop in vapour fraction observed (of the order 10s of seconds rather than 100s). The oscillation seen in Figure 7 could be related to cycles of rapid inflow of air followed by rapid condensation (giving up its heat in a short period, hence reducing the flow), leading to more air being pulled in by the vacuum created (the heat flux decreasing during the period when there is less gas to condense, resulting in an increased flow) until a steady state is created where the inflow rate matches the condensation rate. The oscillation period seen is of the order of 10s of seconds, which would match the observation in the unpublished experiments.

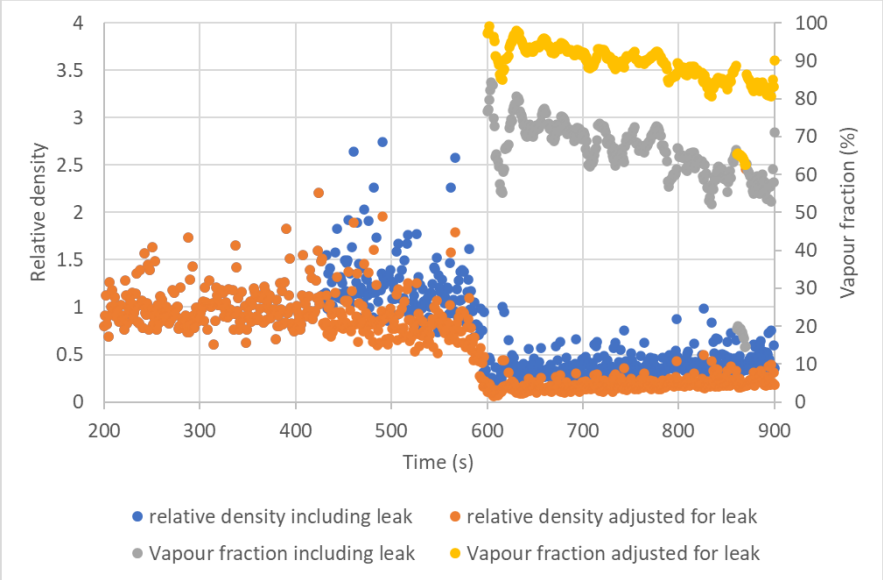

Figure 10: The densities of the fluid relative to that before the leak occurred, and the vapour fraction after loss of vacuum

The heat transfer coefficient is found by estimating the heating rate required to change the fluid density for a given mass flow rate. The first law of thermodynamics for a steady state process undergoing mass transfer and heating is:

$$Q_{in} = \dot{m}(h_{out} - h_{in}) \quad (5)$$

Where in additional to the previously defined variables:

- Q_{in} is the heating rate (J s^{-1})
- h_{in} is the liquid specific enthalpy prior to the leak (J kg^{-1})
- h_{out} is the fluid enthalpy once the vacuum has failed (J kg^{-1})

Where specific enthalpies are evaluated using CoolProp (Bell et al., 2014). The surface heat transfer coefficient (k_{in}, W m$^{-2}K^{-1}$) is then estimated as:

$$k_{in} = \frac{Q_{in}}{\pi D_{\text{pipe}} L_{\text{pipe}} (T_{\text{amb}} - T_{\text{fluid}})} \qquad (6)$$

Table 1: A summary of the values used in the calculations and their results

	Pre vacuum loss	Post vacuum loss Averaged heat transfer		Post vacuum loss Assuming complete evaporation	
		With leak	Without leak	With leak	Without leak
Pressure (barg)	5.5	6	6	6	6
Temperature (K)	25	27	27	27	27
Mass flow (g s^{-1})	150	80	55	80	55
Time (on data logging) (s)	200-400	550-800	550-800	550-800	550-800
Density (kg m^{-3})	65.2	8.71	26.6	5.81	5.81
Vapour fraction (v/v)	0	95	65	100	100
Heat flux (kW m^{-2})	N/A	3.18	7.23	11.1	161
Heat transfer (W m^{-2} K^{-1})	N/A	11.7	26.7	41.1	59.8

Table 1 reports the heat transfer coefficient calculated using the average values and the worst-case scenario of complete evaporation, with values calculated with and without leakage to assess the likely range of values. The heat transfer coefficient when estimated from the experimental data using the average pipe density is found to lie between 11.7 and 26.7 W m^{-2} K^{-1}, for the 80 g s^{-1} and 55 g s^{-1} case respectively. The calculations for the worst-case scenario of complete evaporation shows a likely range between 41 W m^{-2} K^{-1} and 59.8 W m^{-2} K^{-1} for the 80 g s^{-1} and 55 g s^{-1} cases respectively.

For comparison, the transportation pipeline model OLGA typically uses values for uninsulated pipes between 3 W m^{-2} K^{-1} and 5 W m^{-2} K^{-1} for buried pipelines and may choose values up to 50 W m^{-2} K^{-1} for offshore subsea pipeline (Clausen, 2012). PipeTech uses by default 5 W m^{-2} K^{-1} (Yi, 2020), which presumably corresponds to a buried pipeline.

Fesmire (2018) reports heat transfer measurements at various pressures within the vacuum insulation, finding values of approximately 1 W m^{-2} K^{-1} for liquid nitrogen (LN_2) at temperatures where limited air is likely to condense (the temperature of the fluid is above the condensation point of nitrogen but not oxygen). This experiment used a cylindrical cryostat of 168 mm diameter and 1 m length with an LN_2 guard tank at both ends, so approximated a large diameter pipe with no fluid flow.

Other experimental measurements have been made for the deliberate failure of a vacuum in a flexible SIVL containing liquid nitrogen (Demko, 2008). Here, values between approximately[1] 3 W m^{-2} K^{-1} and 45 W m^{-2} K^{-1} are reported, though there are potentially reliability issues with these measurements. For example, the lower value whilst closest to the Fesmire and Johnson value, is disputable due to the possibility that two-phase flow isn't accounted for in the heat transfer calculation which could cause the estimate of the heat transfer value to be artificially reduced. There is also the possibility that the vacuum line insulation was damaged by successive vacuum loss experiments which may have increased the heat transfer. Only two experiments were sufficiently cold for air condensation effects to occur (Runs 3 and 5), and this case corresponded to the highest value (Run 5), however, the subcooling in this case may also have led to the most accurate estimate of the enthalpy change.

It is also likely that the heat transfer values calculated using the average condition underestimate the true value if comparisons to other experiments and the limiting cases of a fully submerged pipeline case are considered. The worst-case

[1] Demko et al. do not explicitly report the ambient temperature, and the value is estimated at approximately 290 K is which is consistent with the values shown in Figure 1. In which case, the temperature change is estimated as 210 K which is sufficiently accurate for modelling purposes here.

scenario of complete evaporation in the pipe provides heat transfer coefficients that likely overestimate the true heat transfer value (see Table 1), though it broadly matches the worst-case values identified in the literature.

To summarise, the calculated heat transfer coefficient is comparable to values that are regularly used in pipeline models, whilst being close to other experimental measurements. Given the unplanned nature of the experiments, there is considerable uncertainty in the estimated heat transfer values. However, considering the paucity of experimental data available, these estimates provide a novel and unexpected insight into a practical vacuum jacket failure event. Future attempts to model pipe vacuum jacket failure should therefore consider using values towards 50 $W\,m^{-2}\,K^{-1}$. A related modelling scenario is that of LH_2 entering warm (uninsulated) pipework, which may induce dramatic pressure rises. In which case, it may be necessary to model the heat loss from the warm pipework using conjugate heat transfer models during the early stages of the release, before using the 50 $Wm^{-2}K^{-1}$ once the pipe wall temperature has cooled sufficiently to not be an easily available source of energy through the walls.

Vacuum loss

It is likely that the vacuum loss in the SIVL was caused by differential contraction of the stainless-steel port and the brass vacuum plug when cooled by LH_2 from the leak on the bayonet coupling. It appears from the increasing flow rate and decreasing vapour fraction that the leak either stopped or slowed as the vapour fraction decreased. There are two plausible mechanisms for this, either the gap between the stalk and vacuum plug started to close up again on further cooling by the LH_2 or a plug of air/water ice formed in the stalk.

Solid/liquid air will have been formed in the outer hose from the cooling by LH_2 flowing through the inner hose after the loss of vacuum. Once the flow of LH_2 was stopped, the system will have warmed up, meaning the solid/liquid air could vaporise, causing a large expansion (around 180 times for liquid to gas at 77 K). This would cause pressurisation of the outer hose, which would push out the vacuum plug at around 0.5 barg. The vacuum plugs in cryogen systems double up as a pressure relieving devices and act like busting disks.

Hazards

The hydrogen being conveyed through the hose was a liquid (or predominantly a liquid) below the saturation temperature prior to the loss of vacuum. Once the vacuum was lost, the hydrogen had increased in temperature and pressure to the saturation point. The fluid being transported through the hose was immediately between 80% and 100% vapour, this decreased over time to between 55% and 88%. If this hydrogen was being used to fill to a tank, then relatively warm saturated vapor will be added rather than colder liquid which was expected. This is a hazard that should be considered when designing the system and the operating procedures.

The largest leak from the bayonet coupling that could be measured was at least 25 g s^{-1} (assuming the leak rate did not continue to increase when the flow dropped off due to loss of vacuum) Using the liquid flow calculation from BS EN IEC 60079-10-1:2021, a flow of 25 g s^{-1} is equivalent to that through a 2.5 mm hole at 5 barg (assuming a discharge coefficient of 0.62).

However, if the video is studied it can be seen that there are several smaller leaks contributing to the release rate, and the fluid flow is split so that it comes out either side of the clamp. The release can be seen to quickly gain buoyancy as it slows down and warms up; the horizontal extent of the cloud appears to be around 2-3 m before rising due to buoyancy. The release looks more similar in extent to the experiment with a 2 g/s release through a 1 mm hole at 6 barg (the visible cloud was around 2.5 m) the release looks to be a series of leaks through holes of the order of 1 mm. Note, the wind was lower for these tests than those they are compared to in the following paragraph.

In comparison, a release of 110 g s^{-1} through an 8 mm nozzle had a visible cloud of around 4 m despite strong cross winds and a release of 200 g s^{-1} through an 8 mm nozzle at 6 barg had a visible cloud in excess of 8 m despite strong cross winds. Strong cross winds would have promoted dilution of the hydrogen cloud, reducing the distance it travels horizontally. It should be noted that the mass flow rates achieved depended on many factors including the temperature of the liquid in the tanker.

Currently, there is little guidance on determining hazardous area classification distances for LH_2 leaks. The 5th Edition of the Energy Institute Model Code of Practice 15 (EI 15) has been updated to included LH_2. The hazardous distance in EI 15 for a 1 mm hole at 5 bara is 5.5 m (for a flow rate of 3 g/s), which is similar to but longer than the visible cloud observed for the 25 g s^{-1} leak from the bayonet coupling.

Hazardous distances have also been calculated using HSE's Quadvent tool (Santon, 2012) as a comparison. Strictly speaking, Quadvent is only applicable for gas releases, but the LH_2 being released has flashed to gas on or before release. The temperature of the gas has been set to be equal to the liquid being released, which is a conservative assumption as it is likely that the gas will warm through contact with the metal and air. Using a 2.5 mm hole in Quadvent, at 5 barg and 25 K gives a distance to LEL of 6 m and to ½ LEL of 12 m (assuming a discharge coefficient of 0.62). Using a 1 mm hole in Quadvent, at 5 barg and 25 K gives a distance to LEL of 2 m and to ½ LEL of 5 m (assuming a discharge coefficient of 0.62). The mass flow rates calculated by the Quadvent software for a gas release give a much lower flow rate than expected for a liquid release but give hazardous distances that are consistent with the 5th Edition of EI 15 and the experiment with the release of LH_2 through a 1 mm hole.

To give a measure of the hazard if all 25 g s^{-1} hydrogen released were ignited, it is compared to the jet fire from a 6 barg LH_2 release through an 8 mm nozzle at 50 g/s, as shown in Figure 11. The jet fire has a horizontal extent of around 8 m.

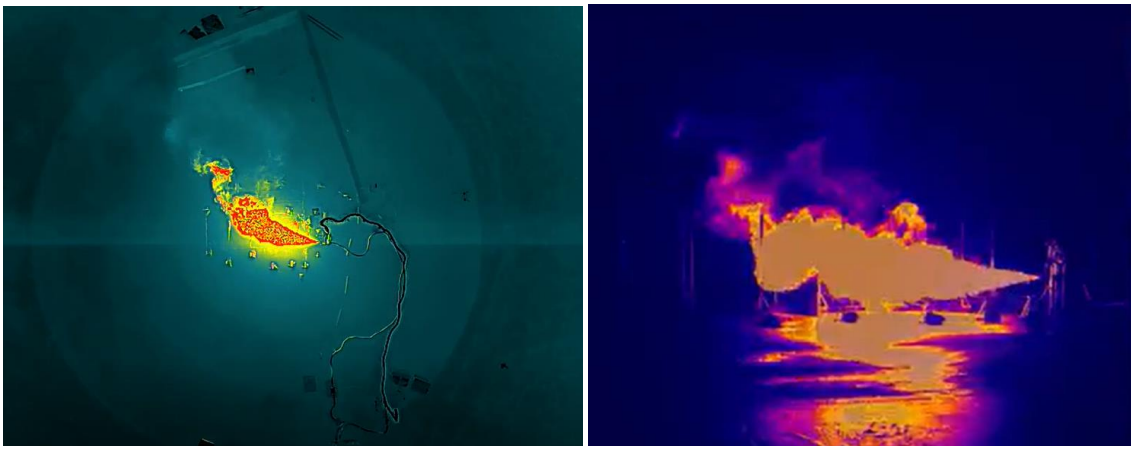

Figure 11: Thermal images of the jet fire from a 6 barg LH2 release through an 8 mm nozzle at 50 g s^{-1}. The test pad the experiment was performed on is 25 m in diameter and the sensor frames span a distance of 8 m. The left picture is an aerial shot from a drone and the right picture taken from the ground looking across the pad. The reflections of the heat flux from the ground can also be seen in the right picture.

Conclusions

A leak of 25 g s^{-1} of LH_2 was measured from a leak on a joint made from a Linde bayonet. Due to the nature of the joint and the clamp holding it together, the leak was more like a circumferential leak or a series of releases from 1 mm holes rather than a single release from a 2.5 mm hole. The hazardous distance horizontally around this leak was estimated as approximately 3 m from the visible extent, which is less than expected from hazardous area classification models such as EI 15 for a release from a 1 mm hole.

This leak impinged on a vacuum port, causing it to leak through differential contraction. The loss of the vacuum caused heating of the LH_2 being flowed through the SIVL, causing it to be raised in pressure by 0.7 barg and temperature by 2 K. The fluid being flowed changed from being predominantly liquid to predominantly vapour at the saturation temperature and pressure. This is a hazard that should be considered when designing LH_2 systems and their operating procedures.

The heat transfer rate was calculated to be between 3.18 and 7.23 kW m^{-2}. The heat transfer coefficient when estimated from the experimental data using the average pipe density is found to lie between 11.7 and 26.7 W m^{-2} K^{-1}. These lie as expected between the limiting cases of buried uninsulated pipelines (3 to 5 W m^{-2} K^{-1}) and subsea uninsulated pipelines (50 W m^{-2} K^{-1}). Given values of 45 W m^{-2} K^{-1} have been observed in other experiments, future attempts to model pipe vacuum jacket failure should therefore consider using values towards 50 W m^{-2} K^{-1}.

Disclaimer

This report and the work it describes were undertaken by the Health and Safety Executive (HSE) under contract to The Aviation Technologies Institute through the ZEST programme. Its contents, including any opinions and/or conclusions expressed or recommendations made, do not supersede current HSE policy or guidance.

References

Bell, I. H., Wronski, J., Quoilin, S., & Lemort, V., 2014, Pure and pseudo-pure fluid thermophysical property evaluation and the open-source thermophysical property library CoolProp. Industrial & engineering chemistry research, 53(6), 2498-2508.

BS EN IEC 60079-10-1:2021, Explosive atmospheres Part 10-1: Classification of areas - Explosive gas atmospheres.

Clausen, S., Oosterkamp, A., and Strøm, K. L., 2012, Depressurization of a 50 km long 24 inches CO2 pipeline. Energy Procedia, 23, 256-265.

Demko J.A., Duckworth R.C, Roden M. and Gouge M., 2008, Testing of a vacuum insulated flexible line with flowing liquid nitrogen during the loss of insulating vacuum, AIP Conf. Proc. 985, 160–167.

Energy Institute, Model code of safe practice Part 15: Area classification for installations handling flammable fluids, 5th edition, 2024.

Fesmire J.E. and Johnson W.L., 2018, Cylindrical cryogenic calorimeter testing of six types of multilayer insulation systems, Cryogenics 89, 58–75.

Funke Th. And Habeestroh Ch., 2015, IOP Conf. Series: Materials Science and Engineering 101, 012058.

Leachman, J.W., Jacobsen, R.T., Penoncello, S.G., and Lemmo,n E.W., Fundamental Equations of State for Parahydrogen, Normal Hydrogen, and Orthohydrogen. J. Phys. Chem. Ref. Data, 38(3):721–748, 2009. doi:10.1063/1.3160306.

Meyer Tool, undated, How cryogenic bayonets work, https://www.mtm-inc.com/how-cryogenic-bayonets-work.html (accessed 05/08/24).

NIST, 2023, Chemistry WebBook, Standard Reference Database, Number 69

Santon R., Ivings M., Webber D. and Kelsey A, 2012, New methods for hazardous area classification for explosive gas atmospheres, Hazards 23.

Sun P.J., Wu J.Y., Zhang P., Xu L. and Jiang M.L., 2009, Experimental study of the influences of degraded vacuum on multilayer insulation blankets, Cryogenics 49, 719–726.

Weinstein, J, 2010, Multiphase Flow in Coriolis Mass Flow Meters – Error Sources and Best Practices, Paper 7.2, 28th International North Sea Flow Measurement Workshop

Yi, J. & Mahgerefteh, H., 2020, An Analytically Based Pressurised Pipeline Decompression Model. Hazards 30 Symposium Series.